Scholar Publishing Group
International Journal of Multimedia Computing
https://doi.org/10.38007/IJMC.2022.030307.
ISSN 2789-7168 Vol. 3, Issue 3: 91-99

Research on Medical CT Intelligent Image Artificial Intelligence Detection System Based on Athletes'core Strength

Tao Zeng, Qianqian Xu, Rong Chen

Medicine College, Jingchu University of Technology, Jingmen 448000, China

200209002@jcut.edu.cn

Keywords: Core Muscle Groups; Improved U-Net; Ct Images; Lstm

Abstract: Current medical evaluations of athletes' core muscle groups lack sufficient quantification. This study employs an improved U-Net architecture to automatically segment core muscle groups in abdominal and lower back CT images of athletes and extracts morphological parameters such as cross-sectional area, muscle density, and fat infiltration rate. Furthermore, by fusing CT morphological parameters with surface electromyography (sEMG) signals, a Long Short-Term Memory (LSTM) network is utilized to predict the core stability index. The system achieves Dice coefficients for automatic segmentation of five types of core muscle groups ranging between 0.84 and 0.92. The AI detection of fat infiltration rate is highly correlated with the pathological gold standard (correlation coefficient 0.976). The root mean square error (RMSE) of the core strength prediction model across five test movements ranges from 0.6 to 1.8, providing a reliable tool for sports injury prevention and training optimization.

1. Introduction

With the increasing demands on athletes' physical fitness and performance in competitive sports, core strength, as a key link in the human kinetic chain, has become a research focus in sports medicine and sports science for its scientific assessment and training optimization. The morphological and functional status of the core muscle groups directly relates to an athlete's stability, power transfer efficiency, and risk of sports injuries.

This paper proposes an athlete core strength assessment system that integrates medical CT intelligent image analysis with artificial intelligence technology. An improved U-Net architecture achieves automatic segmentation of core muscle groups and quantification of morphological parameters. Combined with surface electromyography signals and an LSTM network, a core function prediction model is constructed, ultimately realizing cross-modal correlation analysis from structure to function.

The paper is structured as follows: it reviews the current state of research on imaging and AI

technologies for core strength assessment; elaborates on the methods for core muscle group segmentation, parameter quantification, and function prediction; validates the system's effectiveness through segmentation accuracy, parameter correlation, and prediction error; and Section 5 summarizes the research value and outlines future directions.

2. Related Work

In the field of sports medicine, with continuous technological advancements, various imaging techniques and artificial intelligence methods are widely used for health monitoring and injury diagnosis in athletes. Marano et al. [1] combined clinical presentation and exercise history to explore the application value of CCTA in diagnosing coronary artery abnormalities and clinical management in athletes. Christou et al. [2] retrospectively analyzed clinical data from mature athletes who underwent cardiac CT, including indications, findings, and risk factors related to heart disease, to evaluate the effectiveness and value of cardiac CT in pre-participation screening of athletes. D'Ascenzi et al. [3] reviewed the various applications of cardiac CT in sports cardiology, including anatomical assessment of the athlete's heart, diagnosis of exercise-related cardiovascular diseases, sports risk stratification, and monitoring of cardiac adaptations post-exercise. Ramkumar et al. [4] described the current applications and research progress of artificial intelligence in sports injury diagnosis, rehabilitation, and training. Sarto et al. [5] analyzed the advantages and limitations of ultrasound imaging in muscle and tendon assessment, and how to overcome these limitations to improve its application in elite sports.

Bone stress injuries are common sports injuries among athletes, and magnetic resonance imaging (MRI) is an important tool for assessing the severity and healing of bone stress injuries. Hoenig et al. [6] analyzed the correlation between MRI grading of bone stress injuries and the time for athletes to return to sports. Perrey et al. [7] found that muscle oxygenation measurement technology has broad application potential in sports science, providing important physiological information for sports training and rehabilitation. Guelmami et al. [8] discussed the necessity and importance of establishing ethical guidelines in sports medicine and sports science research practice. McClean et al. [9] found that musculoskeletal injuries in university athletes are not caused by a single factor but by the interaction of multiple factors within the training load, fatigue, and biopsychosocial model. Rhim et al. [10] proposed international recommendations for the application of ESWT in sports medicine, providing guidance for clinicians using ESWT to treat sports-related conditions. Despite numerous advances in athlete health monitoring and injury diagnosis, research on the assessment of athlete core strength and injury prevention requires further depth. This paper aims to provide more scientific and precise technical support for the assessment of core strength and injury prevention in athletes by constructing an AI detection system for medical CT images based on athlete core strength.

3. Methods

3.1 Automatic Segmentation of Core Muscle Groups

To accurately segment various core muscle groups from complex abdominal and lower back CT images, a deep convolutional neural network based on the U-Net architecture is adopted and improved for the specificities of muscle segmentation. The original U-Net shows limitations when processing images with low contrast and blurred boundaries between muscles and surrounding tissues like fat and organs. Therefore, an attention mechanism module is embedded in the skip connections between the encoder and decoder. This module adaptively learns the importance weights of different spatial locations in the feature maps, enabling the network to focus more on the

edges and texture details of muscle tissues when integrating deep and shallow features, thereby enhancing the recognition capability for the contours of deep and small muscles like the paraspinal muscles and transversus abdominis. Simultaneously, residual connections are introduced in the deeper layers of the network to alleviate the gradient vanishing problem in deep networks, ensuring effective network training and learning of richer feature representations. The entire module takes raw CT slices as input and, through end-to-end training, ultimately outputs a probability map of the muscle category for each pixel [11].

3.2 Morphological Parameter Quantification and 3D Modeling

After obtaining high-precision muscle segmentation masks, quantitative morphological parameters are extracted and three-dimensional spatial models are constructed. First, based on the binarized segmentation results, the cross-sectional area of each target muscle group at specific anatomical levels is calculated. Simultaneously, referring back to the Hounsfield Unit values of the original CT images, the pixel value distribution within each muscle group region is statistically analyzed, using its average value as muscle density. The fat infiltration rate is further calculated through specific threshold ranges; this indicator directly reflects the physiological state and health of the muscle. Additionally, a bilateral muscle symmetry analysis algorithm is developed. By calculating the midsagittal plane of the trunk and comparing the cross-sectional area and density of corresponding muscle groups on the left and right sides, the mechanical balance of the athlete's trunk is quantified [12-13]. For more intuitive spatial assessment, utilizing the segmentation results from consecutive CT slices, the marching cubes algorithm is employed for three-dimensional reconstruction, generating a 3D model of the core muscle groups, including intermuscular spaces. This model not only visually displays the volume and spatial relative positions of the muscles but also provides a geometric basis for biomechanical analysis.

Table 1 shows the morphological parameters, including cross-sectional area, muscle density, and fat infiltration rate, obtained through automatic segmentation and quantitative processing for five types of core muscle groups:

Table 1. Quantification Results of Morphological Parameters for Core Muscle Groups

Muscle Type	Cross-sectional Area (cm^2)	Muscle Density (HU)	Fat Infiltration Rate (%)
Transversus Abdominis	15.2	45.3	8.5
Rectus Abdominis	25.6	52.1	6.2
Erector Spinae	35.8	48.7	12.4
Psoas Major	20.4	55.2	9.8
Multifidus	12.7	42.9	15.3

There are significant differences in the morphological parameters of different core muscle groups. The erector spinae has the largest cross-sectional area (35.8 cm^2), while the multifidus has the smallest (12.7 cm^2), reflecting the functional division of labor among different muscles in core stability. Regarding muscle density, the psoas major is the highest (55.2 HU), while the transversus abdominis and multifidus are lower, at 45.3 HU and 42.9 HU respectively, indicating denser muscle tissue in the psoas major, correlating with its key role in trunk flexion and extension. The fat infiltration rate is highest in the multifidus (15.3%) and lowest in the rectus abdominis (6.2%), suggesting that the multifidus is more prone to fatty degeneration, affecting its endurance and recovery capacity. The quantification of these parameters provides a reliable basis for assessing the

structural integrity and functional status of athletes' core muscle groups and helps identify potential injury risks [14].

3.3 Core Strength Function Prediction

To achieve the leap from static structure to dynamic function, a multimodal feature fusion and prediction framework is designed to effectively correlate static CT morphological parameters with dynamic surface electromyography signals. A temporal alignment strategy maps the time points of sEMG signals during specific movement cycles (like flexion-extension, rotation) to the corresponding body posture and muscle state during the CT scan. Subsequently, a multimodal feature fusion module concatenates parameters representing the macrostructure of muscles (cross-sectional area, density, fat infiltration rate) with sEMG features representing the instantaneous activation state of muscles (amplitude, frequency characteristics), forming a comprehensive feature vector containing both structural and functional information. This feature vector is then fed into a Long Short-Term Memory network. Leveraging its strong ability to handle sequential dependencies, the LSTM network learns the complex nonlinear relationships between the morphological basis of different muscles and their activation patterns and force timing during movement sequences [15-16]. Finally, the output layer of this network regresses, through a fully connected layer, two key indicators: a comprehensive core stability index, and a muscle force distribution probability heatmap reflecting the contribution of different muscles during the movement, thereby achieving intelligent and quantitative functional assessment of core strength.

4. Results and Discussion

This study selects medical CT images of the abdomen and lower back from professional athletes and synchronously collected surface electromyography signals as the dataset. The muscle contours and fat infiltration areas are annotated by three radiology experts collectively as the gold standard for analysis. All experiments are run on a workstation equipped with an NVIDIA RTX 3080 GPU, implemented based on the PyTorch framework.

4.1 Automatic Segmentation Accuracy Presentation

The segmentation accuracy of the algorithm on five types of core muscle groups is quantitatively analyzed by calculating the Dice coefficient and Hausdorff distance. Specific experimental results are shown in Figures 1 and 2:

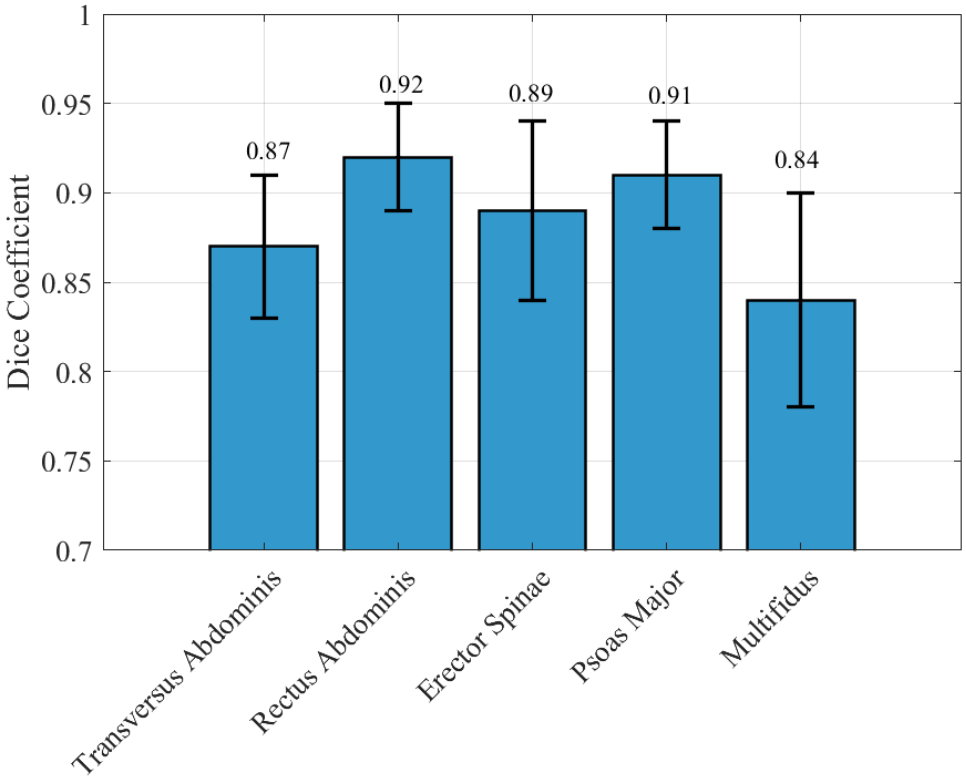

Figure 1. Dice Coefficients for Automatic Segmentation of Core Muscle Groups

The segmentation accuracy for the five types of core muscle groups shows significant differences. The rectus abdominis and psoas major achieve the best segmentation results, with Dice coefficients of 0.92 and 0.91 respectively, while the segmentation accuracy for the multifidus is relatively low, at only 0.84. This difference stems from the unique anatomical characteristics and imaging manifestations of each muscle group. The rectus abdominis, as a superficial muscle, has clear fascial boundaries and uniform density distribution, creating a high contrast with surrounding adipose tissue in CT images, providing ideal conditions for algorithm segmentation. Although the psoas major is deep-seated, its spindle shape and relatively independent anatomical position reduce segmentation difficulty. In contrast, the multifidus, as the deepest stabilizing muscle group alongside the spine, is not only small in volume and complex in shape but also lacks clear anatomical separation from adjacent erector spinae groups. Combined with partial volume effects, this significantly reduces boundary distinguishability. Furthermore, the medium segmentation accuracy for the transversus abdominis and erector spinae reflects an anatomically challenging environment of medium difficulty; the former is limited by the characteristics of thin-layer muscles and interference from respiratory motion artifacts, while the latter faces the challenge of inter-muscular overlap. These results fully demonstrate the adaptability of the improved U-Net architecture in handling segmentation tasks for muscle groups of varying complexity, while also revealing that the segmentation of deep, small muscle groups remains a current technical challenge.

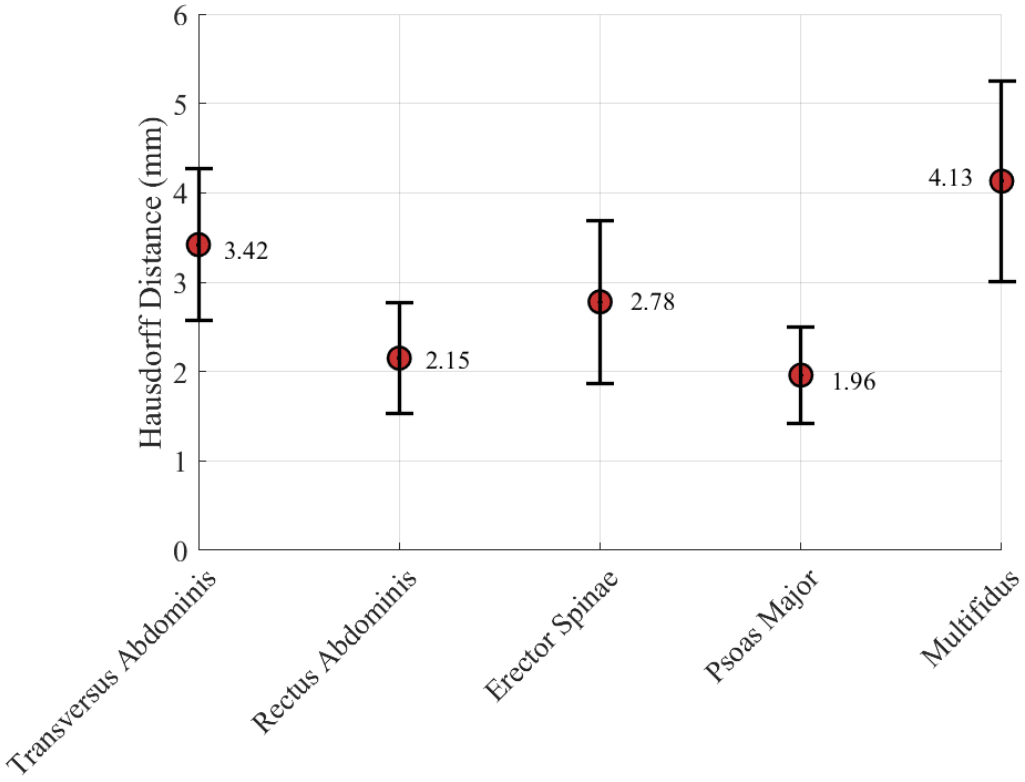

Figure 2. Hausdorff Distance for Core Muscle Group Segmentation

The psoas major shows the best boundary localization accuracy with the smallest Hausdorff distance (1.96 ± 0.54 mm), benefiting from its relatively regular geometric shape and clear muscle-fat interface. The rectus abdominis follows closely (2.15 ± 0.62 mm), its good performance stemming from the clear rectus sheath boundary. In contrast, the multifidus not only has the lowest Dice coefficient but also the largest Hausdorff distance (4.13 ± 1.12 mm), reflecting suboptimal consistency and stability in boundary segmentation for this muscle group, directly related to its complex fan-shaped structure and anatomical characteristic of tight attachment to the vertebral lamina. The medium-level Hausdorff distances for the erector spinae and transversus abdominis (2.78 ± 0.91 mm and 3.42 ± 0.85 mm, respectively) further confirm the positive correlation between segmentation difficulty and structural complexity. The Hausdorff distances for all muscle groups remain within a reasonable range, indicating good robustness of the algorithm across different individuals.

4.2 Validation of Morphological Parameter Quantification Results

Using pathological detection results as the gold standard, abdominal and lower back CT images from 50 athlete samples are collected. The core muscle groups are automatically segmented via the improved U-Net architecture, and the fat infiltration rate is calculated. The AI detection results are compared and analyzed against the pathological gold standard, as shown in Figure 3:

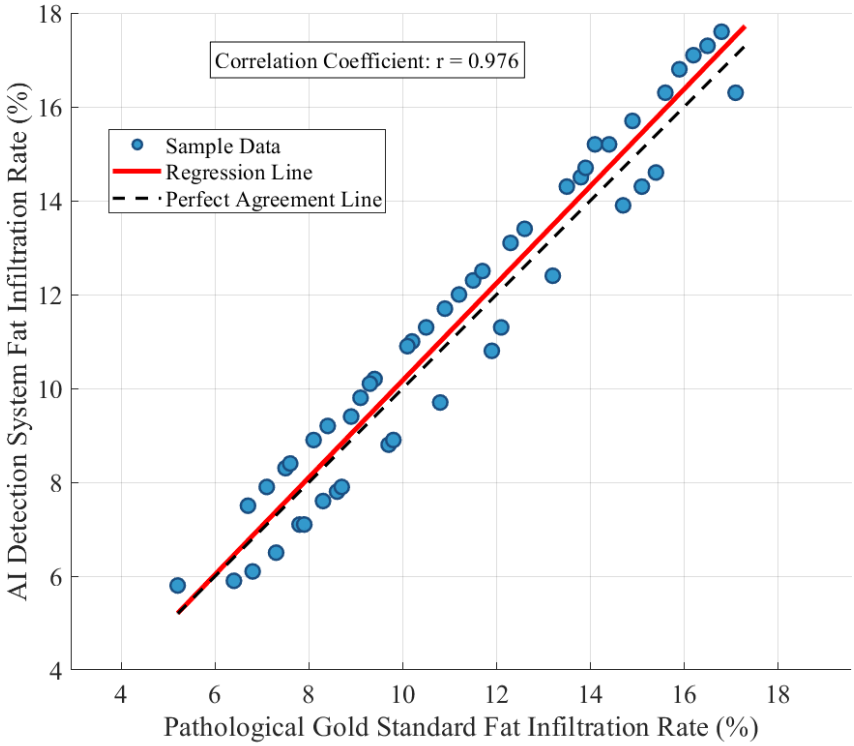

Figure 3. Correlation Analysis between AI-detected Fat Infiltration Rate and Pathological Gold Standard

The correlation analysis results show a high degree of consistency between the AI detection system and the pathological gold standard in the quantitative assessment of fat infiltration rate. The data points in the scatter plot are closely distributed on both sides of the regression line, with a correlation coefficient of 0.976, indicating a strong linear correlation between the two methods. In regions with higher fat infiltration rates (>15%), the data points are slightly more dispersed, reflecting the challenge posed by increased tissue heterogeneity in cases of severe fat infiltration for algorithm recognition. In the medium to low fat infiltration rate range (5%-12%), the data points are more concentrated, showing better detection stability. Overall, the correlation analysis confirms the reliability of the AI system in quantitatively assessing fat infiltration in core muscle groups, providing support for subsequent clinical applications.

4.3 Functional Prediction Model Performance

Five core strength test movements are executed in a standardized laboratory environment: trunk flexion, trunk extension, trunk left rotation, trunk right rotation, and plank. Each movement is repeated 3 times. A Vicon three-dimensional motion capture system (sampling frequency 100 Hz) synchronously captures full-body motion trajectories using 8 MX-T40 cameras, while 2 Bertec force plates (sampling frequency 1000 Hz) record ground reaction force data. The core stability index for biomechanical testing is derived by calculating a weighted composite score of center of gravity sway amplitude and lumbar joint moment variance. Surface electromyography signals are synchronously collected using a Delsys Trigno wireless system (sampling frequency 2000 Hz, bandwidth 20-450 Hz) attached to the muscle belly positions of 5 core muscle groups (transversus abdominis, rectus abdominis, erector spinae, psoas major, multifidus). The sEMG signals are

full-wave rectified and low-pass filtered at 10Hz to extract root mean square and median frequency features. These are temporally aligned with the morphological parameters obtained from CT images and input into the trained LSTM model to predict the core stability index. The predicted values are finally compared with the biomechanical test gold standard, and the root mean square error for each movement is calculated. The results are shown in Table 2:

Table 2. Core Strength Prediction Values vs. Biomechanical Test Results

Test Movement Type	Predicted Core Stability Index	Measured Core Stability Index	Absolute Error	Root Mean Square Error (RMSE)
Trunk Flexion	84.6	83.2	1.4	1.8
Trunk Extension	78.3	79.5	1.2	1.5
Left Trunk Rotation	81.9	82.4	0.5	0.7
Right Trunk Rotation	82.1	81.7	0.4	0.6
Plank	89.8	88.9	0.9	1.1

The functional prediction model demonstrates good predictive performance across all five core strength test movements, with absolute error ranges from 0.4 to 1.4 and root mean square error ranges from 0.6 to 1.8. The model achieves the highest prediction accuracy for rotational movements (left and right rotation), with RMSEs of 0.7 and 0.6 respectively, which is related to the relatively stable synergistic activation patterns of core muscle groups during rotation. The errors are slightly larger for flexion and extension movements, with RMSEs reaching 1.8 and 1.5, originating from the complexity of multi-planar spinal motion in these actions, which increases prediction difficulty. The predicted values maintain high consistency with the measured values across different movement types, confirming that multimodal feature fusion and the LSTM network can effectively capture the intrinsic relationship between the morphological characteristics of core muscle groups and their dynamic function, providing a quantitative basis for athlete core strength assessment.

5. Conclusion

This study constructs an integrated detection system encompassing automatic segmentation of core muscle groups, quantification of morphological parameters, and prediction of core strength function, effectively addressing the pain points of reliance on subjective experience and insufficient quantification in traditional athlete core strength assessment. However, the current model is primarily based on static CT images and sEMG signals collected in laboratory environments, not fully covering the dynamic changes of athletes in real sports scenarios. Furthermore, the sample size is relatively limited, and the model's generalizability across different sports disciplines and athletic levels requires further validation. Future research will focus on expanding sample diversity, incorporating dynamic imaging data, and integrating real-time biomechanical parameter collection during movement using wearable devices to enhance the model's dynamic prediction capability and clinical applicability.

Reference

[1]Marano R, Merlino B, Savino G, et al. Coronary computed tomography angiography in the clinical workflow of athletes with anomalous origin of coronary arteries from the contralateral valsalva sinus[J]. Journal of Thoracic Imaging, 2021, 36(2): 122-130.

[2]Christou G A, Deligiannis A P, Kouidi E J. The role of cardiac computed tomography in pre-participation screening of mature athletes[J]. European journal of sport science, 2022, 22(4): 636-649.

[3]D'Ascenzi F, Baggiano A, Cavigli L, et al. The role of cardiac computed tomography in sports cardiology: back to the future![J]. European Heart Journal-Cardiovascular Imaging, 2022, 23(11): e481-e493.

[4]Ramkumar P N, Luu B C, Haeberle H S, et al. Sports medicine and artificial intelligence: a primer[J]. The American Journal of Sports Medicine, 2022, 50(4): 1166-1174.

[5]Sarto F, Spörri J, Fitze D P, et al. Implementing ultrasound imaging for the assessment of muscle and tendon properties in elite sports: practical aspects, methodological considerations and future directions[J]. Sports medicine, 2021, 51(6): 1151-1170.

[6]Hoenig T, Tenforde A S, Strahl A, et al. Does magnetic resonance imaging grading correlate with return to sports after bone stress injuries? A systematic review and meta-analysis[J]. The American Journal of Sports Medicine, 2022, 50(3): 834-844.

[7]Perrey S, Quaresima V, Ferrari M. Muscle oximetry in sports science: an updated systematic review[J]. Sports Medicine, 2022, 54(4): 975-996.

[8]Guelmami N, Ben Ezzeddine L, Hatem G, et al. The ethical compass: establishing ethical guidelines for research practices in sports medicine and exercise science[J]. International Journal of Sport Studies for Health, 2022, 7(2): 31-46.

[9]McClean Z J, Pasanen K, Lun V, et al. A biopsychosocial model for understanding training load, fatigue, and musculoskeletal sport injury in university athletes: a scoping review[J]. The Journal of Strength & Conditioning Research, 2021, 38(6): 1177-1188.

[10]Rhim H C, Singh M, Maffulli N, et al. Recommendations for use of extracorporeal shockwave therapy in sports medicine: an international modified Delphi study[J]. British journal of sports medicine, 2021, 59(18): 1287-1301.

[11]Palmisano A, Darvizeh F, Cundari G, et al. Advanced cardiac imaging in athlete's heart: Unravelling the grey zone between physiologic adaptation and pathology[J]. La radiologia medica, 2021, 126(12): 1518-1531.

[12]Jamshidi A M, Soldozy S, Levi A D. Percutaneous direct pars repair in young athletes[J]. Neurosurgery, 2022, 92(2): 263-270.

[13]Chowdhury P N, Shivakumara P, Raghavendra R, et al. An episodic learning network for text detection on human bodies in sports images[J]. IEEE Transactions on Circuits and Systems for Video Technology, 2021, 32(4): 2279-2289.

[14]Samet J D. Pediatric sports injuries[J]. Clinics in sports medicine, 2021, 40(4): 781-799.

[15]Miro P, Crawford A, Mills M K, et al. Imaging of primary periphyseal finger stress injuries in climbers[J]. Skeletal Radiology, 2022, 54(6): 1215-1224.

[16]Soligard T, Palmer D, Steffen K, et al. New sports, COVID-19 and the heat: sports injuries and illnesses in the Tokyo 2020 Summer Olympics[J]. British journal of sports medicine, 2021, 57(1): 46-54.